Polymer Chemistry

Accepted Manuscript

ROYAL SOCIETY OF CHEMISTRY

www.rsc.org/polymers

Photoinduced Topological Transformation of Cyclized Polylactides for Switching the Properties of Homocrystals and Stereocomplexes†

Naoto Sugai, Shigeo Asai,* Yasuyuki Tezuka,* and Takuya Yamamoto*

Department of Organic and Polymeric Materials, Tokyo Institute of Technology

O-okayama, Meguro-ku, Tokyo 152–8552, Japan

E-mail: asai.s.aa@m.titech.ac.jp, ytezuka@o.cc.titech.ac.jp yamamoto.t.ay@m.titech.ac.jp;

Fax +81 3 5734 2876

†Electronic supplementary information (ESI) available: Fig. S1–9 and Table S1.

Cyclized poly($_L$-lactide) and poly($_D$-lactide) (M_n ~3 kDa) incorporating an *o*-nitrobenzyl group as a photocleavable linker were synthesized and photoirradiated for topological transformation to form photocleaved linear polylactides. By DSC, T_m of the cyclized stereocomplex (167 °C) decreased by more than 40 °C from that of the linear prepolymers (209 °C) despite their essentially identical molecular weights. Upon the photocleavage, the resulting linear stereocomplex showed almost same T_m (211 °C) as that before the cyclization. The enthalpy of melting of crystals having an infinite thickness, i.e.,

ΔH_m(100%), and the surface free energy (σ_e) were determined by the combination of WAXD, SAXS, and DSC. Both ΔH_m(100%) and σ_e were considerably smaller for the cyclized polylactide homocrystals and stereocomplexes compared to those of the linear prepolymers and photocleaved products. These suggest that the absolute enthalpy of the melt state is lower, and the crystal–amorphous interface is more stable for the cyclized polylactides arising from the topology.

Introduction

Stimuli-responsive polymers have attracted great interest and been developed for numerous applications.[1] For example, poly(*N*-isopropylacrylamide) is known for a thermal responsive polymer that shows a lower critical solution temperature at around 32 °C by dehydration.[2] pH-Responsive polymers are often employed for lithography[3] and drug delivery system (DDS)[4] by taking advantage of switching their solubility through deprotection and (de)protonation. Furthermore, DDS[5] and self-healing materials[6] using redox-responsive polymers were reported. However, these responses require a stimulus on essentially every monomer unit, and thus a considerable amount of heat, acid/base, or oxidant/reductant, is indispensible. In order to establish a notably more efficient

stimuli-responsive polymer system, we expected that cyclic polymers have a substantial potential because only one cleaving reaction per polymer molecule leads to the cyclic-to-linear topological transformation to trigger changes in the properties. Furthermore, the molecular weight and chemical structure of the main chain are unaffected through the topological transformation. In this relation, cyclic polymers were reported to give significantly enhanced material properties compared to relevant linear polymers, including the stability of micelles.[7]

The reversible linear–cyclic topological transformation of polystyrene and poly(ethylene oxide) was reported by making use of thiol–disulfide conversion,[8] hydrogen bonding,[9] and the dimerization of porphyrin.[10] In addition, the photocleavage of cyclic morpholino[11, 12] and oligonucleotide[13] were sometimes employed to control gene expression. Nevertheless, topological transformation has never been applied to stimuli-responsive polymeric materials.

We previously synthesized cyclic poly($_L$-lactide), PLLA, (**2L**) and poly($_D$-lactide), PDLA, (**2D**) (number average molecular weight (M_n) ~3 kDa, Figure 1a), as well as cyclic stereoblock polylactides, and reported the melting points (T_m) of their homocrystals and stereocomplexes[14, 15] using differential scanning calorimetry (DSC).[16] The linear and cyclic

stereocomplexes showed distinguishable T_m, and we expected that this stereocomplex system can be applied for a topology-dependent stimuli-responsive polymeric material. Meanwhile, Waymouth and co-workers reported DSC, wide-angle X-ray diffraction (WAXD), and small-angle X-ray scattering (SAXS) of cyclic PLLA and PDLA having a relatively large molecular weight (≥ 26 kDa) synthesized by zwitterionic ring-opening polymerization.[17] These cyclic polylactides exhibited similar thermal and crystallographic properties to their linear counterparts. In regard to this, polylactide stereocomplexes is known to form folded chain crystals for the molecular weights larger than several thauthands.[18] The folded chain crystals likely resulted in diminished and/or complicated influences by the polymer topology. In addition, the optical purity of these cyclic polylactides was modest due to the partial racemization during the ring-expansion polymerization.

In the present work, cyclic PLLA and PDLA with M_n of approximately 3 and 1.5 kDa incorporating an *o*-nitrobenzyl group (NB) as a photocleavable linker[19] were synthesized via highly optically pure polymerization (Figure 1b). These homopolymers and their stereocomplexes were subjected to WAXD, SAXS, and DSC measurements to study the effects of the polymer topology on the extended chain crystals. Furthermore, the

cyclic-to-linear topological transformation by photoirradiation was performed. T_m of the stereocomplex, which decreased upon cyclization by 42 °C (T_m before the cyclization, 209 °C; T_m after the cyclization, 167 °C), restored to 211 °C by the photocleavage. The difference in T_m arose from the crystal thickness (l_c) in the lamellar structure,[20] directly reflecting the topology of the polymers. Furthermore, The enthalpy of melting of crystals having an infinite thickness, i.e., $\Delta H_m(100\%)$, and the surface free energy (σ_e) of the crystalline layers were significantly smaller for the homocrystals and stereocomplex of the cyclic polylactides. Coupled with the recently attracted bio-based, bio-degradable, and carbon-neutral features of polylactides, the switch of the properties by the topological transformation should find various applications.

Results and Discussion

Synthesis of photocleavable cyclic PLLA (5L) and PDLA (5D) with a NB group. A NB group, which is one of the most widely used photolabile protecting groups due to its prompt removal, was chosen as the photocleavable linker.[19] The cyclic-to-linear topological transformation was expected to be enabled by the molecular design that incorporates the photocleavable NB linker in the main chain of the cyclic polymers (Figure

1c). Cyclic PLLA (**5L**) and PDLA (**5D**) with a photocleavable linker were prepared using a similar method to that of **2L** and **2D**, which were reported previously (Figures 1a and 1b).[16] In this regard, the employed polymerization is known to form highly optically pure polylactide without degradation in the stereochemistry.[21] The intermediate and final products were fully characterized using ^{1}H NMR, SEC, and MALDI-TOF MS (Figures S1–S3).

Photocleavage. To achieve selective photoinduced cyclic-to-linear topological transformation, the conditions for the photocleavage reaction were investigated. The photoirradiation experiments were first conducted with the most available linear polylactides with the photocleavable linker at the chain end (**3L** and **3D**) under various conditions to form **7L** and **7D**, respectively (Figure 1d). The experiments were performed using a wavelength of 365 nm and an intensity of 700 mW/cm^2.[19] Polylactide has a very weak absorption at 365 nm; the main chain should not be directly decomposed by the photoirradiation.[22] Good solvents for polylactide homopolymers in the absence of absorption around 365 nm such as CH_2Cl_2, $CHCl_3$, THF, toluene, CH_3CN, 1,2-dichloroethane, and EtOAc were used.[22] At a polymer concentration of 0.5 mg/mL, 30 min of irradiation caused decomposition and crosslink of the main chains, as observed by

SEC for all of these solvents (Figure S4). The photocleavage of the NB group generated unstable nitroso compounds, which spontaneously collapsed to form radicals, leading to the radical-mediated degradation of the polylactide main chain.[19] Therefore, a radical scavenger (butylated hydroxytoluene, BHT) was added, and the decomposition and crosslink were found to be effectively suppressed (Figure S4b bottom).

On the basis of these results, the photocleavage of cyclic **5L** and **5D** was investigated. The SEC traces after photoirradiation (**6L** and **6D**) in the presence of BHT exhibited suppression of the main chain degradation (Figure S5). The photocleavage was observed after 2 h by noticeable peak top shifts toward the smaller elution volume. The peak molecular weight of **6L** (M_p = 5.0 kDa), which represented the hydrodynamic volume, was nearly equal to that of linear prepolymer **4L** (M_p = 5.2 kDa), in agreement with previously reported linearization reactions.[8, 23] Moreover, the SEC trace of **6L** also has a shoulder peak at M_p = 11 kDa, which is comparable to that of a dimer of **6L** (2 × 5.0 kDa = 10 kDa). A similar shoulder also appeared in **6D** (Figure S5). The dimers presumably formed by the intermolecular coupling of the nitroso groups, which were resulted by the photocleavage (Figure S6).[24] During the photocleavage process, the nitroso group remained at the terminus of the polylactide chains and likely formed the dimer by the nitroso–nitroso

association.[25] Furthermore, trimer or higher multimer formation was not detected, suggesting the dimerization occurred through this mechanism. This hypothesis was also supported by the photocleavage reaction of linear PLLA possessing a NB group (**3L**) in Figure S4. The dimerization of photocleaved **3D** in the presence of BHT was not observed because **3D** had a molecular structure to detach the nitroso group from the main chain upon the photocleavage (Figure 1d). By comparing the ^{1}H NMR spectra of **5L** and **6L**, the signals for the NB group ("f" at 6.38–6.46 ppm, "d" at 6.91 ppm, and "e" at 7.63 ppm) clearly decreased after photoirradiation (Figure S7). The small peaks remained in the aromatic region of **6L** could be due to the nitroso–nitroso association products.[25] A decrease of signal "o" in **6L** (Figure S7) suggests that this photocleavage process is accompanied by some other side reactions on the alkene due to the reactivity of the intermediate radicals and/or nitroso group. Based on these results, it was concluded that the cyclic-to-linear topological transformation was successfully completed. The photocleavage in the solid state was also studied. Despite many attempts under various conditions, the decomposition of the polylactides occurred before the completion of the intended photocleavage reaction. Thus, the solid-state topological conversion is currently investigated.

X-ray structures. The X-ray structural analysis of the solvent-cast samples of the

previously reported non-photocleavable linear and cyclic polylactides without a NB group (**1L**, **1D**, **2L**, **2D**, **1L/1D**, **1L/2D**, and **2L/2D**)[16] was first conducted. The WAXD profiles of individual **1L**, **1D**, **2L**, and **2D** showed diffraction peaks at 2θ = 15, 17, 19° that are ascribed to the α- or α'-forms of the polylactides homocrystals (Figure S8, left).[26] The degree of crystallinity (χ_c) of the homocrystals was estimated by the profiles (**1L**, 63%; **1D**, 58%; **2L**, 64%; **2D**, 50%). Figure S8 (right) shows the WAXD profiles of the enantiomeric blends of **1L/1D**, **1L/2D**, and **2L/2D**. The diffraction peaks at 2θ = 12, 21, and 24° are attributed to stereocomplex.[26] The χ_c values of the stereocomplexes were also estimated (**1L/1D**, 79%; **1L/2D**, 62%; **2L/2D**, 69%).

The SAXS profiles of the individual polymers (**1L**, **1D**, **2L**, and **2D**) and the blends (**1L/1D**, **1L/2D**, and **2L/2D**) are shown in Figure S9. The values of the long spacing (L), i.e., the distance between the centers of adjacent crystallites, the crystal thickness (l_c), and the thickness of the amorphous intercrystalline layers (l_a) of **1L** (L = 12 nm, l_c = 8.2 nm, l_a = 2.1 nm), **1D** (L = 12 nm, l_c = 9.4 nm, l_a = 2.5 nm), **2L** (L = 6.3 nm, l_c = 3.9 nm, l_a = 2.4 nm), and **2D** (L = 6.1 nm, l_c = 3.6 nm, l_a = 2.5 nm) were determined (Table S1).[27] The direction of the thickness of the polylactide homocrystals is the same as the c axis of the unit cell, which is 2.886 nm consisting of ten lactic acid units.[28] Thus, based on

above-mentioned l_c, the number of lactic acid units and its molecular weight in the crystal layers were: **1L**, 28 units for M_n = 2.0 kDa; **1D**, 33 units for M_n = 2.3 kDa, **2L**, 14 units for M_n = 1.0 kDa, and **2D**, 12 units for M_n = 0.9 kDa (Table S1). On the basis of M_n determined by NMR (~3 kDa), these results suggest that linear **1L** and **1D** form extended chain crystals with the residual lengths of the polymer chains existing in the amorphous layers (Figure 2a).[29] In the case of **2L** and **2D**, the polymer chain supposedly formed the flattened conformation shown in Figure 2b, and thus, l_c became nearly half that of **1L** and **1D**.[30] Furthermore, the SAXS peak became dull for cyclized **2L** and **2D** (Figure S9). This indicates that the crystal lattice was distorted likely due to the difficulty in the alignment of the polymer chains restricted by the cyclic topology.

The SAXS profiles of the enantiomeric blends are also shown in Figure S9, and the values of L, l_c and l_a were estimated (**1L/1D**, L = 12 nm, l_c = 10 nm, l_a = 2.1 nm; **1L/2D**, L = 8.8 nm, l_c = 7.2 nm, l_a = 1.6 nm; **2L/2D**, L = 7.0 nm, l_c = 5.4 nm, l_a = 1.6 nm) as shown in Table S1.[27] The direction of the thickness of a polylactide stereocomplex is the same as the c axis of the unit cell, which is 0.87 nm consisting of three lactic acid units.[18, 31, 32] Thus, based on the above-mentioned l_c, the number of lactic acid units and the molecular weights in the crystal layers were: **1L/1D**, 34 units for M_n = 2.5 kDa; **1L/2D**, 25 units for M_n = 1.8

kDa, and **2L/2D**, 17 units for M_n = 1.3 kDa (Table S1). Given that M_n ~3 kDa, these results suggest that, similar to the homocrystals, **1L/1D** forms extended chain crystals with the residual lengths of the polymer chains existing in the amorphous layers (Figure 2a). In the case of **2L/2D** (l_c = 5.4 nm), the polymer chains form the flattened conformation shown in Figure 2b, and thus, l_c became nearly half that of **1L/1D** (l_c = 10 nm).[30] In the case of the linear/cyclic blend (**1L/2D**), the L and l_c values were in between the linear/linear and cyclic/cyclic blends.

The newly synthesized photocleavable linear and cyclic PLLA and PDLA (**4L**, **4D**, **5L**, and **5D**) were subsequently subjected to the WAXD and SAXS measurements. Although **4L**, **4D**, **5L**, and **5D** possess the photocleavable linker, the crystallographic properties of these polylactides were relevant to those without the photocleavable linker (**1L**, **1D**, **2L**, and **2D**). The WAXD showed diffraction peaks at 2θ = 15, 17, 19° that are ascribed to the α- or α'-forms of polylactide homocrystals (Figure 3).[26] The χ_c values of these samples were estimated from the profiles (**4L**, 62%; **4D**, 60%; **5L**, 58%; **5D**, 56%) as in Table 1. The SAXS profiles are shown in Figure 4, and L, l_c, and l_a were determined: **4L** (L = 13 nm, l_c = 9.3 nm, l_a = 3.6 nm), **4D** (L = 13 nm, l_c = 8.6 nm, l_a = 4.0 nm), **5L** (L = 7.5 nm, l_c = 4.8 nm, l_a = 2.7 nm), and **5D** (L = 8.1 nm, l_c = 5.3 nm, l_a = 2.8 nm). Therefore, L

and l_c of cyclic **5L** and **5D** were considerably smaller compared with linear **4L** and **4D** (Figure 2),[27] similar to the polylactides without the photocleavable linker.[30] The molecular weights of the polylactide units in the crystalline layers were also calculated (Table 1).

The WAXD peaks at 2θ = 12, 21, 24 °, attributing to a stereocomplex, were observed for **4L/4D**, **4L/5D**, and **5L/5D** (Figure 3).[26] Additional diffractions at 2θ = 13 and 18 ° were detected for the stereocomplexes involving the cyclic polylactides (**4L/5D** and **5L/5D**). We assume that the photocleavable linker in the cyclic polymer that is incorporated in the crystalline layer caused these diffractions (Figure 2b). In contrast, the photocleavable linker in the linear polymers, which was attached at the chain end, was presumably in the amorphous layer (Figure 2a). Based on the WAXD profiles, the χ_c values of the stereocomplexes were estimated as shown in Table 1 (**4L/4D**, 69%; **4L/5D**, 54%; **5L/5D**, 61%). In this relation, the linear/linear blends showed several percent higher χ_c values than the cyclic/cyclic blends for both photocleavable (**4L/4D**, 69%; **5L/5D**, 61%) and non-photocleavable (**1L/1D**, 79%; **2L/2D**, 69%) polylactides. The χ_c value for the linear/cyclic blends was lowest (**4L/5D**, 54%; **1L/2D**, 62%) likely due to the difficulty of crystallization arising from the unmatched topologies of the enantiomeric pairs. By comparing the lamellar structures estimated from the SAXS profiles of **4L/4D** (L = 12 nm,

l_c = 9.4 nm, l_a = 2.5 nm) and **5L/5D** (L = 7.6 nm, l_c = 5.1 nm, l_a = 2.4 nm) (Table 1), a significant decrease of L and l_c due to the cyclization was revealed. Therefore, the polylactides possessing a photocleavable linker (**4L**, **4D**, **5L**, and **5D**) and their blends have similar effects on the crystallographic properties via cyclization[30] as the polylactides without a photocleavable linker (**1L**, **1D**, **2L**, and **2D**) and their blends.

Lastly, the photoirradiated PLLA/PDLA blend (**6L/6D**) was also subjected to the WAXD and SAXS measurements. The crystal form was unchanged; the diffraction peaks at 2θ = 12, 21, and 24 ° in the WAXD profile (Figure 3) were ascribed to the stereocomplex. The χ_c value was estimated to be 49% (Table 1). The additional peaks at 2θ = 13 and 18 °, which were found in cyclic/cyclic **5L/5D** before the photocleavage as well as in linear/cyclic **4L/5D**, disappeared indicating that theses diffractions were indeed from the photocleavable units in the crystalline layers. Despite the same crystal form determined by WAXD, SAXS revealed an increase of L and l_c upon the photoirradiation. The estimated values for **6L/6D** (L = 15 nm, l_c = 13 nm) were more than double in comparison with those of **5L/5D** (L = 7.6 nm, l_c = 5.1 nm) (Table 1), indicating that the cyclic polymers were photocleaved to likely form extended chain crystals (Figure 2). When compared with **4L/4D** (L = 12 nm, l_c = 9.4 nm), those for **6L/6D** were found to be significantly larger. This

is probably because of some degree of the dimerization through the nitroso–nitroso association occurred (Figure S6).[25] The number of lactic acid units and their molecular weight in the crystal layers were 45 units and M_n = 3.2 kDa, respectively. Furthermore, l_a for both homocrystals and stereocomplexes was relatively large for the polylactides containing the photocleavable linker (**4L**, **4D**, **5L**, **5D**, **4L/4D**, **4L/5D**, and **5L/5D**) compared with those without the photocleavable linker including the one after the photocleavage (**1L**, **1D**, **2L**, **2D**, **1L/1D**, **1L/2D**, **2L/2D** and **6L/6D**), as shown in Tables 1 and S1. These results were likely due to the volume of the photocleavable linkers in the amorphous layer. Moreover, the SAXS peak of photocleaved **6L/6D** was somewhat sharpened in comparison with that of cyclic **5L/5D** (Figure 4), suggesting the order of the crystal lattice is restored to some extent after the photocleavage.

Melting points (T_m). The T_m values of the non-photocleavable linear and cyclic polylactides were previously reported.[16] In the present study, those of the linear and cyclic polylactides with a photocleavable linker and the photocleaved stereocomplex were measured by DSC to investigate the effects of the topological conversion. The homocrystals of linear **4L** and **4D** had T_m of 142 °C, whereas cyclic **5L** and **5D** showed lowered T_m of 128 and 125 °C, respectively (Table 1, Figure 5).[15] The blend of linear

4L/4D showed T_m of 209 °C, which was higher than the respective homopolymers due to typical stereocomplexation.[15, 33] In contrast, the blends involving a cyclic polylactide showed relatively low T_m values: **4L/5D**, 173 °C; **5L/5D**, 167 °C. Notably, the effect of cyclization was more prominent for the stereocomplexes (T_m(**5L/5D**) – T_m(**4L/4D**) = –42 °C) than for the homocrystals (T_m(**5L**) – T_m(**4L**) = –14 °C; T_m(**5D**) – T_m(**4D**) = –17 °C). After the photocleavage, T_m of **6L/6D** increased to 211 °C, which was more than 40 °C higher than that of cyclized **5L/5D** (167 °C) and comparable to that before the cyclization (**4L/4D**, 209 °C). These results suggest that T_m of the stereocomplexes of the present polylactides is switchable by approximately 40 °C through controlling their polymer topology.

Enthalpies of melting (ΔH_m, ΔH_m(100%)). The ΔH_m values were calculated from the DSC thermograms (Figure 5) and converted to those for crystals having an infinite thickness, i.e., ΔH_m(100%), based on the crystallinity determined by WAXD (Figure 3).[34] Interestingly, we found that the homocrystals consisting of a cyclic polymer (**5L** and **5D**) have significantly smaller ΔH_m(100%) (44 J/g) than those of the linear counterparts (**4L**, 60 J/g; **4D**, 68 J/g) as shown in Table 1. This difference presumably arose from the absolute enthalpy of the respective melt states rather than those of the crystalline states because the

line widths of the WAXD peaks, thus crystallite size and lattice distortion, were comparable (Figure 3). In other words, the absolute enthalpy of cyclic **5L** and **5D** in the melt state is expected to be lower by roughly 20 J/g than that of linear **5L** and **5D** due to the topology. In this relation, linear polymers are relatively easy to entangle in the melt state, possibly leading to the higher absolute enthalpy, while cyclic polymers are less likely.[35] Moreover, the ΔH_m(100%) values of the present polylactides (**4L**, 60 J/g; **4D**, 68 J/g; **5L**, 44 J/g; **5D**, 44 J/g) were much smaller than those used for PLLA with high molecular weights (100 and 135 J/g for linear PLLA (M_n(PS) = 360–450 kDa, where M_n(PS) indicates that M_n determined by SEC calibrated using standard PS) as shown in Table 1.[36] Presumably, this was also caused by the high degree of entanglement in the melt state due to the length of the polymers. The trend for the ΔH_m(100%) values of the stereocomplexes is parallel to that of the homocrystals; the cyclic/cyclic blend (**5L/5D**, 43 J/g) as well as the linear/cyclic blend (**4L/5D**, 41 J/g) has notably smaller ΔH_m(100%) than the linear/linear blend (**4L/4D**, 87 J/g) and that after the photocleavage (**6L/6D**, 89 J/g). In addition, the ΔH_m(100%) value for a stereocomplex calculated based on the previous report using longer PLLA (M_v = 27 kDa) and PDLA (M_v = 25 kDa)[34] was also considerably larger (146 J/g).

Furthermore, photocleavable linear PLLA (**4L'**), linear PDLA (**4D'**), cyclic PLLA

(**5L'**), and cyclic PDLA (**5D'**) with molecular weight of approximately 1.5 kDa were also synthesized and subjected to DSC measurements in order to study the molecular weight dependence. No T_m was found for any these individual polylactides likely due to the insufficient length for crystallization. However, the blends of linear/linear **4L'/4D'**, cyclic/cyclic **5L'/5D'**, and photocleaved **6L'/6D'** had T_m of 138, 127, and 155 °C with ΔH_m of 29, 6, and 16 J/g, respectively. This trend concerning the polymer topology is same for the polylactides with a molecular weight of approximately 3 kDa, but lower T_m and smaller ΔH_m were likely due to the smaller molecular weight.

Surface free energy (σ_e). σ_e of the interface between the crystal and amorphous was calculated by the Gibbs–Thomson equation (1) using the reported values of the densities (homocrystal, 1.285 g/cm^3;[37] stereocomplex, 1.27 g/cm^3)[32, 38] and equilibrium melting points, $T_m°$ (homocrystal, 215 °C;[39] stereocomplex, 279 °C).[40]

$$T_m(l_c) = T_m° \times [1 - 2\sigma_e/(\Delta H_m(100\%) \times l_c)] \quad (1)$$

The σ_e value for linear **4L** (54 mJ/m^2) and **4D** (55 mJ/m^2) was close to that of high-molecular-weight linear PLLA (M_n(PS) = 360–450 kDa[36] (52–64 mJ/m^2)), which has the chain-folding surfaces of the crystalline layers. On the other hand, σ_e for cyclic **5L** (24 mJ/m^2) and **5D** (28 mJ/m^2) was significantly smaller. This suggests that cyclic **5L** and **5D**

form a well-ordered looped structure at the crystal surfaces (Figure 2b) to help stabilizing the crystal–amorphous interface compared to linear **4L** and **4D** having chain ends (Figure 2a). On the other hand, the folding segments of high-molecular-weight PLLA were probably not as organized as those of cyclic **5L** and **5D**, resulting in the high σ_e values (52–64 mJ/m^2). The less ordered folding segments of high-molecular-weight PLLA are also suggested by the thicker amorphous layers (l_a = 11.9–20.6 nm in Table 1). The higher stability of the interface was also determined for the stereocomplex of cyclic **5L/5D** (28 mJ/m^2) compared to linear **4L/4D** (66 mJ/m^2) and the reported blend of linear PLLA (M_v = 27 kDa) and PDLA (M_v = 25 kDa) (66 mJ/m^2).[34] The linear/cyclic blend of **4L/5D** (35 mJ/m^2) was comparable to cyclic/cyclic **5L/5D** (28 mJ/m^2). On the other hand, considerably higher σ_e was found for photocleaved **6L/6D** (91 mJ/m^2), probably caused by the ununiform chemical structure of the photoreacted chain ends and/or the partial intermolecular coupling through the nitroso–nitroso association.

Interestingly, Müller and coworkers studied the crystallization of linear and cyclic poly(ε-caprolactone) and found that higher T_m and larger σ_e for the cyclic polymers,[41] opposing to the present results of the polylactides. The different crystal systems were expected to cause the opposite *topology effects* from the respective polymers. For reference,

they also reported that higher spherulitic growth rates for cyclic poly(ε-caprolactone) than linear analogues.[41, 42] Conversely, cyclic poly(tetrahydrofuran)[43] and cyclic polyethylene[44] showed a slower rate than their linear counterparts. Presumably, the higher growth rate for cyclic poly(ε-caprolactone) was due the faster diffusion.[45] On the other hand, the unfavorable entropic process governed the crystallization of cyclic poly(tetrahydrofuran) and cyclic polyethylene, resulting in the slower rates. The elucidation of the relationship between the polymer topology and T_m and σ_e of these crystal systems is strongly desired and currently in progress.

Conclusions

Photocleavable cyclic PLLA and PDLA possessing a NB group were synthesized and subjected to a photocleavage reaction to transform the topology. The WAXD and SAXS measurements of the present polylactides, along with previously reported non-photocleavable polylactides, were performed. Despite WAXD indicated that the essentially crystallographically identical homocrystals and stereocomplexes are formed by the linear and cyclic polylactides, SAXS of the cyclic polylactides showed that L and l_c are roughly half of the linear counterparts due to the flattened ring conformation. Moreover, the

photocleaved PLLA/PDLA blend showed L and l_c values comparable to those before the cyclization. DSC showed that T_m of the stereocomplex reflects l_c; more than 40 °C of T_m was controlled through the linear–cyclic topological transformation. The combination of WAXD, SAXS, and DSC revealed that $\Delta H_m(100\%)$ is smaller for the homocrystals and stereocomplex of the cyclic polylactides compared to the respective linear counterparts. Furthermore, the interface between the crystal and amorphous phases was significantly more stable for the cyclic polylactides shown by smaller σ_e.

The present results provide new insights into the structure and properties of crystalline polymeric materials. Novel designs based on the cyclic polymer topology and simple photoirradiation would lead to versatile control on the properties such as T_m, $\Delta H_m(100\%)$, and σ_e, which cannot be achieved by traditional means. Moreover, a photocleavage reaction to increase T_m by approximately 40 °C is appropriate for the efficient processing of polylactide materials. Taking together, the present methodology is expected to lead to the development of novel topology-based stimuli-responsive materials, which require only one reaction per polymer molecule and allow for switching the properties without altering the chemical structure and molecular weight of the polymer.

Experimental Section

Materials. Unless otherwise noted, all commercial reagents were used as received. 3-Buten-1-ol (>98.0%, Tokyo Chemical Industry Co., Ltd.) was distilled prior to use. $_{L}$-lactide (>99%, Musashino Chemical Laboratory, Ltd.) and $_{D}$-lactide (>99%, Musashino Chemical Laboratory, Ltd.) were recrystallized from dry toluene twice prior to use. According to the previously reported procedure,[11] 1-(4,5-dimethoxy-2-nitro-phenyl)-but-3-ene-1-ol was prepared. THF (>99.0%, Kanto Chemical Co., Inc.) was distilled over Na wire. Toluene (>99%, Godo Co., Inc.) was distilled over CaH_2. For column chromatography, Wakosil C-300 (Wako Pure Chemical Industries, Ltd.) was used. SiliaMetS® DMT (SiliCycle Inc.) was used to remove the residue of the second-generation Hoveyda–Grubbs catalyst. Synthesis was repeated several times for some polymers, resulting in different (although slight) M_n, M_p, and PDI values for such polymers.

Synthesis of α-NB-ω-hydroxy-PLLA (3L) and α-NB-ω-hydroxy-PDLA (3D). A vacuum-dried mixture of $_{L}$-lactide (7.00 g, 49 mmol), tin(II) 2-ethylhexanoate (5.6 mg, 14 μmol), and 1-(4,5-dimethoxy-2-nitro-phenyl)-but-3-ene-1-ol (615 mg, 2.4 μmol) was heated at 130 °C for 3 h under nitrogen atmosphere.[46] The reaction mixture was allowed to

cool to ambient temperature and reprecipitated from CH_2Cl_2 into MeOH to yield **3L** (M_n(NMR) = 3.2 kDa, M_p(SEC) = 4.6 kDa, PDI = 1.16) as white solid in 98% conversion. Likewise, **3D** (M_n(NMR) = 3.2 kDa, M_p(SEC) = 4.3 kDa, PDI = 1.17) was synthesized using $_D$-lactide in 98% conversion. ^{1}H NMR: δ (ppm) 1.41–1.76 (m, –$CO_2CH(CH_3)$–), 2.47–2.80 (m, 2H, –$CH_2CH{=}CH_2$), 3.98 (t, 6H, J = 7.7, Ar–OCH_3), 4.35 (q, 1H, J = 6.8 Hz, –$CH(CH_3)OH$), 5.06–5.36 (m, –$CO_2CH(CH_3)$–, –$CH{=}CH_2$), 5.76–5.92 (m, 1H, –$CH{=}CH_2$), 6.45–6.51 (m, 1H, Ar–C*H*–), 6.94 (d, 1H, J = 24.6 Hz, Ar–*H* ortho to N), 7.64 (d, 1H, J = 15.0 Hz, Ar–*H* meta to N).

Synthesis of α-NB-ω-ethenyl-PLLA (4L) and α-NB-ω-ethenyl-PDLA (4D). To a dry THF solution (280 mL) of a mixture of **3L** (1.00 g, 0.31 mmol), 1-(3-dimethylaminopropyl)-3-ethylcarbodiimide hydrochloride (EDAC, 2.11 g, 11 mmol), and 4-dimethylaminopyridine (DMAP, 1.34 g, 11 mmol) was added 4-pentenoic acid (1.32 g, 13 mmol), and the resulting suspension was refluxed for 20 h under nitrogen atmosphere.[47] The reaction mixture was evaporated to dryness under reduced pressure, and the residue was dissolved in CH_2Cl_2. The organic phase was washed with aqueous HCl (0.2 N) and saturated aqueous $NaHCO_3$, dried over anhydrous Na_2SO_4, and evaporated to dryness under reduced pressure. The residue was reprecipitated from CH_2Cl_2 into MeOH to

allow isolation of **4L** (769 mg, M_n(NMR) = 3.2 kDa, M_p(SEC) = 5.2 kDa, PDI = 1.10) as light brown solid in 77% yield. Likewise, **4D** (M_n(NMR) = 3.2 kDa, M_p(SEC) = 5.0 kDa, PDI = 1.11) was synthesized using **3D** in 88% yield. ^{1}H NMR: δ (ppm) 1.40–1.77 (m, –$CO_2CH(CH_3)$–), 2.33–2.79 (m, 6H, CH_2=CHCH_2CH–, CH_2=CHCH_2CH_2CO_2–), 3.98 (t, 6H, J = 7.7, Ar–OCH_3), 5.06–5.37 (m, –CO_2CH(CH_3)–, –CH=CH_2), 5.76–5.90 (m, 1H, –CH=CH_2), 6.45–6.51 (m, 2H, Ar–CH–), 6.94 (d, 1H, J = 24.9 Hz, Ar–H ortho to N), 7.64 (d, 1H, J = 14.4 Hz, Ar–H meta to N).

Synthesis of photocleavable cyclic PLLA (5L) and photocleavable cyclic PDLA (5D). To a toluene (1.0 L) solution of **4L** (200 mg, 53 μmol) was added a toluene solution (2 mL) of the second-generation Hoveyda–Grubbs catalyst (132 mg, 0.11 mmol), and the resulting solution was stirred at 80 °C for 48 h.[16, 48] Ethyl vinyl ether (20 mL) was added, and the mixture was stirred at ambient temperature for 3 h. The reaction mixture was evaporated to dryness, and the residue was subjected to column chromatography (SiO_2, CH_2Cl_2/MeOH 500/4 vol/vol) followed by stirring with SiliaMetS® DMT to remove the catalyst residue to give crude **5L** (M_p(SEC) = 3.5 kDa). The crude polymer was fractionated using preparative SEC to allow isolation of **5L** (166 mg, M_n(NMR) = 3.0 kDa, M_p(SEC) = 3.3 kDa) in 83% yield. Likewise, **5D** (M_n(NMR) = 3.1 kDa, M_p(SEC) = 3.5 kDa) was

synthesized using **4D** in 88% yield. ^{1}H NMR: δ (ppm) 1.40–1.75 (m, –$CO_2CH(CH_3)$–), 2.28–2.92 (m, 6H, –CH_2CH_2CH=$CHCH_2$–), 3.97 (t, 6H, J = 4.2, Ar–OCH_3), 4.98–5.33 (m, –$CO_2CH(CH_3)$–), 5.48–5.56 (s, 2H, –CH=CH–), 6.38–6.46 (m, 1H, Ar–CH–), 6.91 (d, 1H, J = 23.1 Hz, Ar–*H* ortho to N), 7.63 (d, 1H, J = 14.4 Hz, Ar–*H* meta to N).

Photocleavage Reaction. Photocleavable polylactides (**3L**, **3D**, **5L**, **5D**, or **5L/5D**) were dissolved in CH_2Cl_2, $CHCl_3$, THF, toluene, CH_3CN, 1,2-dichroloethane, or EtOAc. To the solution, was added butylated hydroxy toluene (BHT, 0.05%) where applicable. The solution was photoirradiated at 365 nm using an Asahi Spectra POT-365 light source to form **7L**, **7D**, **6L**, **6D**, or **6L/6D**, respectively.

Measurements. ^{1}H NMR spectra were recorded at ca. 20 °C on a JEOL JNM-AL300 spectrometer operating at 300 MHz. $CDCl_3$ was used as a solvent, and the proton chemical shifts were reported relative to the signal of tetramethylsilane. SEC measurements were performed at 40 °C on a Tosoh model CCPS equipped with a TSK G3000HXL column and a refractive index detector model RI 8020. $CHCl_3$ was used as an eluent at a flow rate of 1.0 mL/min. Linear polystyrene standards were used for calibration, and M_p of a sample was reported as a linear polystyrene equivalent. MALDI–TOF mass spectra were recorded on a Shimadzu AXIMA Performance spectrometer equipped with a

nitrogen laser (λ = 337 nm). The spectrometer was operated at an accelerating potential of 20 kV in a linear positive ion mode with pulsed ion extraction. A CH_2Cl_2 solution (3.0 μL) of a polymer sample (1.0 mg/mL), an acetone solution (3.0 μL) of *trans*-2-[3-(4-*tert*-butylphenyl)-2-methyl-2-propylidene]malonitrile (DCTB) (10 mg/mL), and an acetone solution (3.0 μL) of sodium trifluoroacetate (10 mg/mL) were deposited onto a sample target plate in sequence. Mass values were calibrated using the four-point method using peaks from SpheriCal®, monodisperse dendritic calibration standards that had *m*/*z* = 1715.68, 2255.88, 2796.08, and 3422.35 for polymers in a molecular weight range of 1200–3800 and *m*/*z* = 3636.44, 4816.89, 5997.34, and 7263.87 for polymers in a molecular weight range of 3400–8000. SEC fractionation was performed on a JAI LC-908 equipped with JAIGEL-2H and JAIGEL-3H columns, and $CHCl_3$ was used as an eluent at a flow rate of 3.5 mL/min. WAXD measurements were performed on a Rigaku RINT-2100 spectrometer with CuKa radiation (λ = 0.15418 nm) operating at 40 kV and 40 mA. The optical system with a pinhole geometry consisted of a graphite monochromator and scintillation counter. The intensity data were collected in the 2θ range between 3 and 60 °. SAXS measurements were conducted on a Rigaku NANO-Viewer system with CuKα radiation (λ = 0.15418 nm) operating at 40 kV and 20 mA. The SAXS intensity measured

by pin-hole collimation was corrected for parasitic scattering. The intensity data were collected in the 2θ range between 0.1 and 2.5 °. A powder sample was filled in the center space of a 0.8-mm-thick stainless folder and sealed both faces with amorphous polyethylene thin films of less than 10-μm thickness. DSC measurements were performed on a Seiko DSC 6200, and all samples were cast from CH_2Cl_2 solutions. Thermograms were recorded during the first heating cycle at a rate of 5 or 10 °C/min under a nitrogen gas flow of 50 mL/min.

Acknowledgements

The authors are grateful to Prof. M. Kakimoto and Prof. T. Hayakawa for access to measurement facilities. This work was supported by Grant-in-Aid for JSPS Fellows (23·9581, N.S.), Grants for Excellent Graduate Schools (N.S.), and KAKENHI (26288099 T.Y).

References

1 (a) M. A. C. Stuart, W. T. S. Huck, J. Genzer, M. Muller, C. Ober, M. Stamm, G. B. Sukhorukov, I. Szleifer, V. V. Tsukruk, M. Urban, F. Winnik, S. Zauscher, I. Luzinov

and S. Minko, *Nat. Mater.*, 2010, **9**, 101-113; (b) J. F. Mano, *Adv. Eng. Mater.*, 2008, **10**, 515-527; (c) X. Yan, F. Wang, B. Zheng and F. Huang, *Chem. Soc. Rev.*, 2012, **41**, 6042-6065.

2 H. G. Schild, *Prog. Polym. Sci.*, 1992, **17**, 163-249.

3 Y. N. Xia and G. M. Whitesides, *Annu. Rev. Mater. Sci.*, 1998, **28**, 153-184.

4 D. Schmaljohann, *Adv. Drug Delivery Rev.*, 2006, **58**, 1655-1670.

5 M. Huo, J. Yuan, L. Tao and Y. Wei, *Polym. Chem.*, 2014, **5**, 1519-1528.

6 M. Nakahata, Y. Takashima, H. Yamaguchi and A. Harada, *Nat. Commun.*, 2011, **2**, 511.

7 (a) S. Honda, T. Yamamoto and Y. Tezuka, *J. Am. Chem. Soc.*, 2010, **132**, 10251-10253; (b) S. Honda, T. Yamamoto and Y. Tezuka, *Nat. Commun.*, 2013, **4**, 1574.

8 M. R. Whittaker, Y.-K. Goh, H. Gemici, T. M. Legge, S. Perrier and M. J. Monteiro, *Macromolecules*, 2006, **39**, 9028-9034.

9 (a) O. Altintas, P. Gerstel, N. Dingenouts and C. Barner-Kowollik, *Chem. Commun.*, 2010, **46**, 6291-6293; (b) O. Altintas, E. Lejeune, P. Gerstel and C. Barner-Kowollik, *Polym. Chem.*, 2012, **3**, 640-651.

10 (a) M. Schappacher and A. Deffieux, *J. Am. Chem. Soc.*, 2011, **133**, 1630-1633; (b) M. Schappacher and A. Deffieux, *Macromolecules*, 2011, **44**, 4503-4510.

11 S. Yamazoe, I. A. Shestopalov, E. Provost, S. D. Leach and J. K. Chen, *Angew. Chem. Int. Ed.*, 2012, **51**, 6908-6911.

12 Y. Wang, L. Wu, P. Wang, C. Lv, Z. Yang and X. Tang, *Nucleic. Acids. Res.*, 2012, **40**, 11155-11162.

13 (a) L. Wu, Y. Wang, J. Wu, C. Lv, J. Wang and X. Tang, *Nucleic. Acids. Res.*, 2013, **41**, 677-686; (b) J. C. Griepenburg, B. K. Ruble and I. J. Dmochowski, *Bioorg. Med. Chem.*, 2013, **21**, 6198-6204.

14 (a) K. Fukushima and Y. Kimura, *Polym. Int.*, 2006, **55**, 626-642; (b) M. Kakuta, M. Hirata and Y. Kimura, *Polym. Rev.*, 2009, **49**, 107-140; (c) L. Yu, K. Dean and L. Li, *Prog. Polym. Sci.*, 2006, **31**, 576-602.

15 H. Tsuji, *Macromol. Biosci.*, 2005, **5**, 569-597.

16 N. Sugai, T. Yamamoto and Y. Tezuka, *ACS Macro Lett.*, 2012, **1**, 902-906.

17 E. J. Shin, A. E. Jones and R. M. Waymouth, *Macromolecules*, 2012, **45**, 595-598.

18 H. Marubayashi, T. Nobuoka, S. Iwamoto, A. Takemura and T. Iwata, *ACS Macro Lett.*, 2013, **2**, 355-360.

19 (a) C. G. Bochet, *J. Chem. Soc., Perkin Trans.*, *1* 2002, 125-142; (b) H. Zhao, E. S. Sterner, E. B. Coughlin and P. Theato, *Macromolecules*, 2012, **45**, 1723-1736.

20 H. D. Keith, in *Physics and Chemistry of the Organic Solid State,* ed. D. Fox, M. M. Labes and A. Weissberger, Interscience Publishers, New York, 1963, vol. 1, pp. 462-542.

21 S. J. Huang and J. M. Onyari, *J. Macromol. Sci., Pure Appl. Chem.*, 1996, **A33**, 571-584.

22 R. Auras, B. Harte and S. Selke, *Macromol. Biosci*., 2004, **4**, 835-864.

23 M. M. Stamenović, P. Espeel, E. Baba, T. Yamamoto, Y. Tezuka and F. E. Du Prez, *Polym. Chem.*, 2013, **4**, 184-193.

24 K. G. Orrell, V. Šik and D. Stephenson, *Magn. Reson. Chem.*, 1987, **25**, 1007-1011.

25 (a) R. R. Holmes, R. P. Bayer, L. A. Errede, H. R. Davis, A. W. Wiesenfeld, P. M. Bergman and D. L. Nicholas, *J. Org. Chem.*, 1965, **30**, 3837-3840; (b) J. Li and Q. Wang, *J. Polym. Sci., Part A: Polym. Chem.*, 2014, **52**, 810-815.

26 (a) L. Bouapao, H. Tsuji, K. Tashiro, J. Zhang and M. Hanesaka, *Polymer*, 2009, **50**, 4007-4017; (b) H. Tsuji, T. Wada, Y. Sakamoto and Y. Sugiura, *Polymer*, 2010, **51**, 4937-4947.

27 (a) L. B. Li, Z. Y. Zhong, W. H. de Jeu, P. J. Dijkstra and J. Feijen, *Macromolecules*, 2004, **37**, 8641-8646; (b) M. Fujita, T. Sawayanagi, H. Abe, T. Tanaka, T. Iwata, K. Ito, T. Fujisawa and M. Maeda, *Macromolecules*, 2008, **41**, 2852-2858; (c) L. Chang and E. M. Woo, *Macromol. Chem. Phys.*, 2011, **212**, 125-133.

28 (a) W. Hoogsteen, A. R. Postema, A. J. Pennings, G. ten Brinke and P. Zugenmaier, *Macromolecules*, 1990, **23**, 634-642; (b) K. Wasanasuk and K. Tashiro, *Polymer*, 2011, **52**, 6097-6109.

29 H. Takeshita, M. Poovarodom, T. Kiya, F. Arai, K. Takenaka, M. Miya and T. Shiomi, *Polymer*, 2012, **53**, 5375-5384.

30 G.-E. Yu, T. Sun, Z.-G. Yan, C. Price, C. Booth, J. Cook, A. J. Ryan and K. Viras, *Polymer*, 1997, **38**, 35-42.

31 L. Cartier, T. Okihara and B. Lotz, *Macromolecules*, 1997, **30**, 6313-6322.

32 D. Sawai, Y. Tsugane, M. Tamada, T. Kanamoto, M. Sungil and S. H. Hyon, *J. Polym. Sci., Part B: Polym. Phys.*, 2007, **45**, 2632-2639.

33 Y. Ikada, K. Jamshidi, H. Tsuji and S. H. Hyon, *Macromolecules*, 1987, **20**, 904-906.

34 H. Tsuji, F. Horii, M. Nakagawa, Y. Ikada, H. Odani and R. Kitamaru,

Macromolecules, 1992, **25**, 4114-4118.

35 M. Kapnistos, M. Lang, D. Vlassopoulos, W. Pyckhout-Hintzen, D. Richter, D. Cho, T. Chang and M. Rubinstein, *Nat. Mater.*, 2008, **7**, 997-1002.

36 H. Tsuji, K. Ikarashi and N. Fukuda, *Polym. Degrad. Stab.*, 2004, **84**, 515-523.

37 T. Miyata and T. Masuko, *Polymer*, 1997, **38**, 4003-4009.

38 (a) J. Kobayashi, T. Asahi, M. Ichiki, A. Oikawa, H. Suzuki, T. Watanabe, E. Fukada and Y. Shikinami, *J. Appl. Phys.*, 1995, **77**, 2957-2973; (b) J. Puiggali, Y. Ikada, H. Tsuji, L. Cartier, T. Okihara and B. Lotz, *Polymer*, 2000, **41**, 8921-8930.

39 B. Kalb and A. J. Pennings, *Polymer*, 1980, **21**, 607-612.

40 H. Tsuji and Y. Ikada, *Macromol. Chem. Phys.*, 1996, **197**, 3483-3499.

41 H.-H. Su, H.-L. Chen, A. Díaz, M. T. Casas, J. Puiggalí, J. N. Hoskins, S. M. Grayson, R. A. Pérez and A. J. Müeller, *Polymer*, 2013, **54**, 846-859.

42 (a) R. A. Pérez, M. E. Córdova, J. V. López, J. N. Hoskins, B. Zhang, S. M. Grayson and A. J. Müller, *React. Funct. Polym.*, 2014, **80**, 71-82; (b) M. E. Córdova, A. T. Lorenzo, A. J. Müller, J. N. Hoskins and S. M. Grayson, *Macromolecules*, 2011, **44**, 1742-1746.

43 Y. Tezuka, T. Ohtsuka, K. Adachi, R. Komiya, N. Ohno and N. Okui, *Macromol.*

Rapid Commun., 2008, **29**, 1237-1241.

44 T. Kitahara, S. Yamazaki and K. Kimura, *Kobunshi Ronbunshu*, 2011, **68**, 694-701.

45 H. Takeshita and T. Shiomi, in *Topological Polymer Chemistry: Progress of Cyclic Polymers in Syntheses, Properties and Functions*, ed. Y. Tezuka, World Scientific, Singapore, 2013, pp. 317-328.

46 (a) J. Watanabe, T. Eriguchi and K. Ishihara, *Biomacromolecules*, 2002, **3**, 1109-1114; (b) H. Shinoda and K. Matyjaszewski, *Macromolecules*, 2001, **34**, 6243-6248.

47 T. Yamamoto, T. Fukushima, Y. Yamamoto, A. Kosaka, W. Jin, N. Ishii and T. Aida, *J. Am. Chem. Soc.*, 2006, **128**, 14337-14340.

48 Y. Tezuka and R. Komiya, *Macromolecules*, 2002, **35**, 8667-8669.

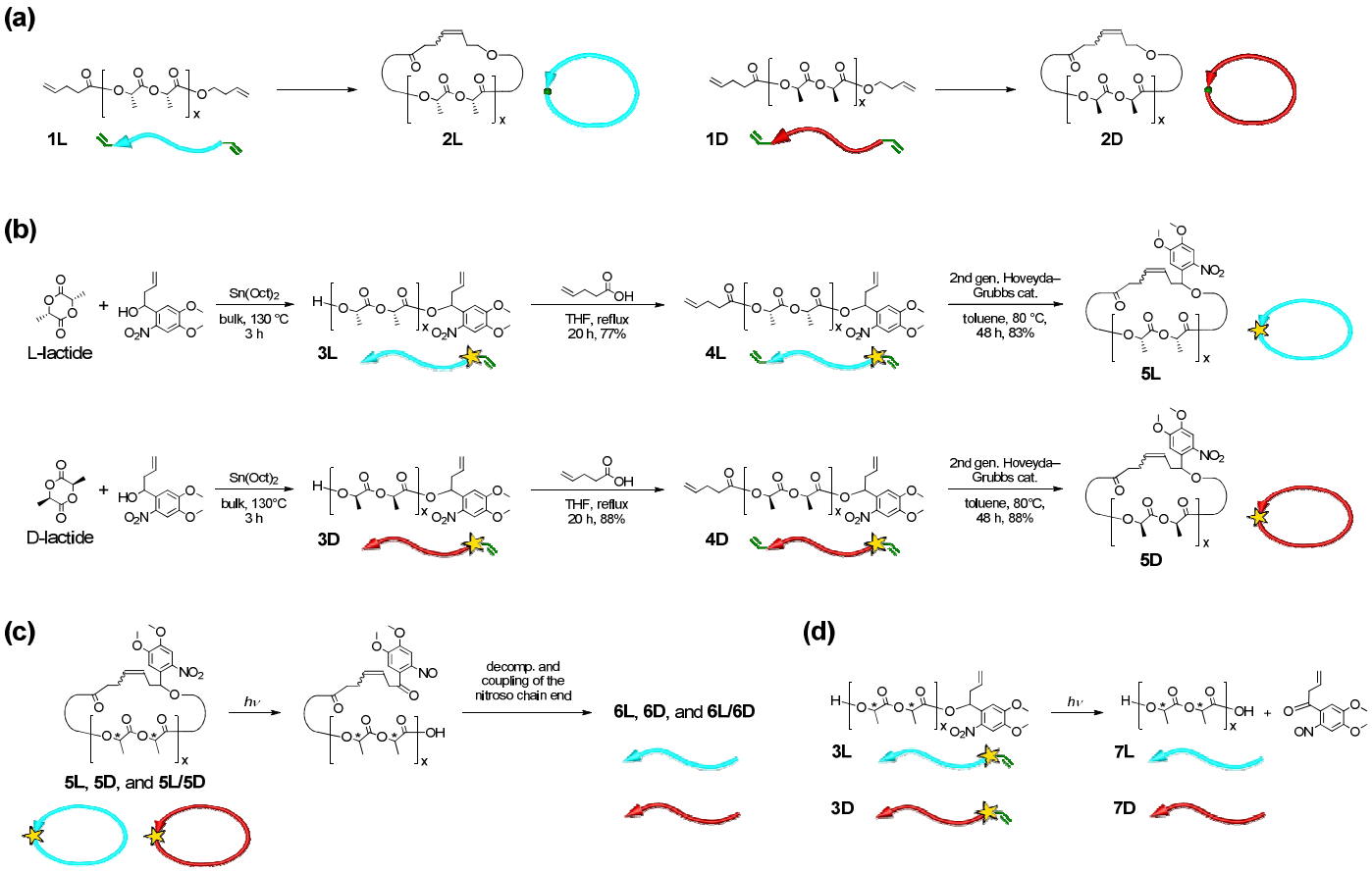

Figure 1. Chemical structures and schematic representation of linear and cyclic PLLA and PDLA used in the present study. (a) Non-photocleavable **1L**, **2L**, **1D**, and **2D**. (b) Synthetic scheme for photocleavable **3L**, **4L**, **5L**, **3D**, **4D**, and **5D**. (c) Photocleavage of **5L**, **5D**, and their blend (**5L/5D**) to Form **6L**, **6D**, and **6L/6D**, respectively. (d) Photocleavage of **3L** and **3D** to form **7L** and **7D**, respectively. For convenience, the direction of the polylactide main chains is indicated by an arrow; the head of the arrows indicates the hydroxyl end, and the tail of the arrows indicates the carboxylic acid end. PLLA and PDLA are shown in light blue and red, respectively. The yellow stars indicate a photocleavable NB linker.

Table 1. Properties of photocleavable linear and cyclic polylactides determined by SAXS, WAXD, and DSC

	description	L (nm)	l_c (nm)	M_n for l_c (kDa)	l_a (nm)	χ_c	T_m (°C)	ΔH_m (J/g)	ΔH_m(100%) (J/g)	σ_e (mJ/m^2)
4L	photocleavable linear PLLA (M_n ~ 3 kDa)	13	9.3	2.3	3.6	62%	142	37	60	54
4D	photocleavable linear PDLA (M_n ~ 3 kDa)	13	8.6	2.1	4.0	60%	142	41	68	55
5L	photocleavable cyclic PLLA (M_n ~ 3 kDa)	7.5	4.8	1.2	2.7	58%	128	26	44	24
5D	photocleavable cyclic PDLA (M_n ~ 3 kDa)	8.1	5.3	1.3	2.8	56%	125	25	44	28
	linear PLLA (M_n(PS) = 360–450 kDa[a])	22.2–35.1[a]	7.6–19.6[a]	1.9–4.9[b]	11.9–20.6[a]	34.2%–55.8%[a]	176.5–190.1[a]	46.2–55.8[a]	100,[a] 135[a]	52–64[b]
4L/4D	blend of **4L** and **4D**	12	9.4	2.3	2.5	69%	209	60	87	66
4L/5D	blend of **4L** and **5D**	10	7.0	1.7	3.1	54%	173	22	41	35
5L/5D	blend of **5L** and **5D**	7.6	5.1	1.3	2.4	61%	167	26	43	28
6L/6D	photoirradiated **5L/5D**	15	13	3.2	1.5	49%	211	44	89	91
	blend of linear PLLA (M_v = 27 kDa) and PDLA (M_v = 25 kDa)[c]	12.0[c]	8.2[c]	2.0[d]	3.8[c]	70%[c]	231[c]	102[c]	146[d]	66[d]

[a] Values reported in Tsuji, H.; Ikarashi, K.; Fukuda, N. *Polym. Degrad. Stab.* **2004**, *84*, 515–523.[36]

[b] Values calculated based on those reported in Tsuji, H.; Ikarashi, K.; Fukuda, N. *Polym. Degrad. Stab.* **2004**, *84*, 515–523.[36]

[c] Values reported in Tsuji, H.; Horii, F.; Nakagawa, M.; Ikada, Y.; Odani, H.; Kitamaru, R. *Macromolecules* **1992**, *25*, 4114–4118.[34]

[d] Values calculated based on those reported in Tsuji, H.; Horii, F.; Nakagawa, M.; Ikada, Y.; Odani, H.; Kitamaru, R. *Macromolecules* **1992**, *25*, 4114–4118.[34]

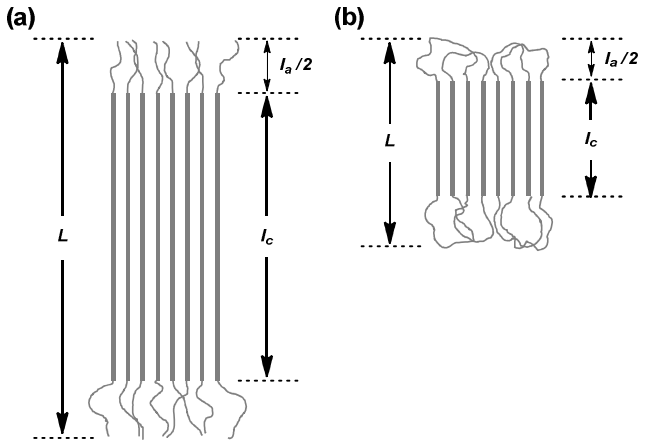

Figure 2. Schematic representation of the lamellar structures of (a) linear and (b) cyclic homocrystals and stereocomplexes of the polylactides determined by SAXS. *L*, long period; I_a, amorphous thickness; I_c, crystal thickness.

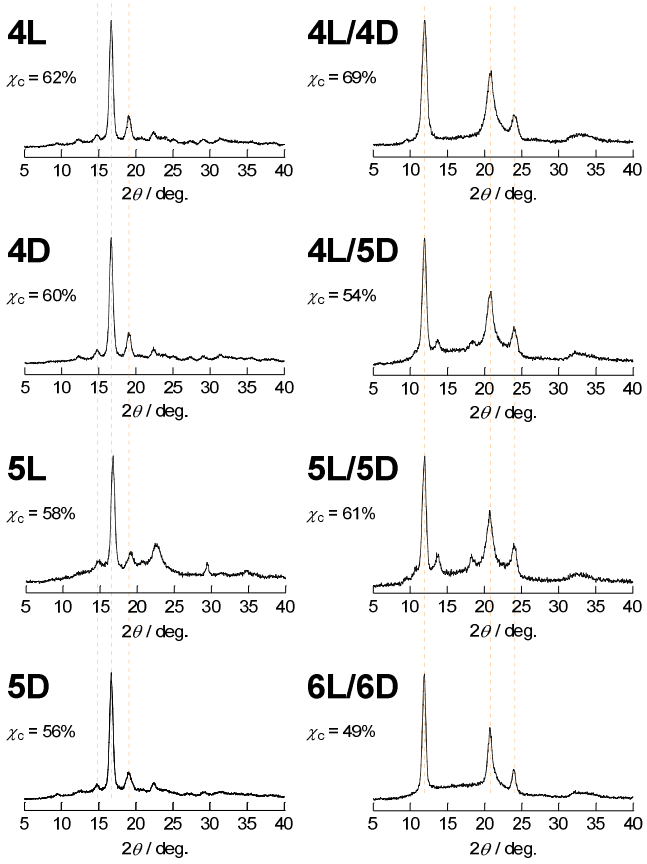

Figure 3. WAXD profiles of **4L**, **4D**, **5L**, **5D**, **4L/4D**, **4L/5D**, **5L/5D**, and **6L/6D**.

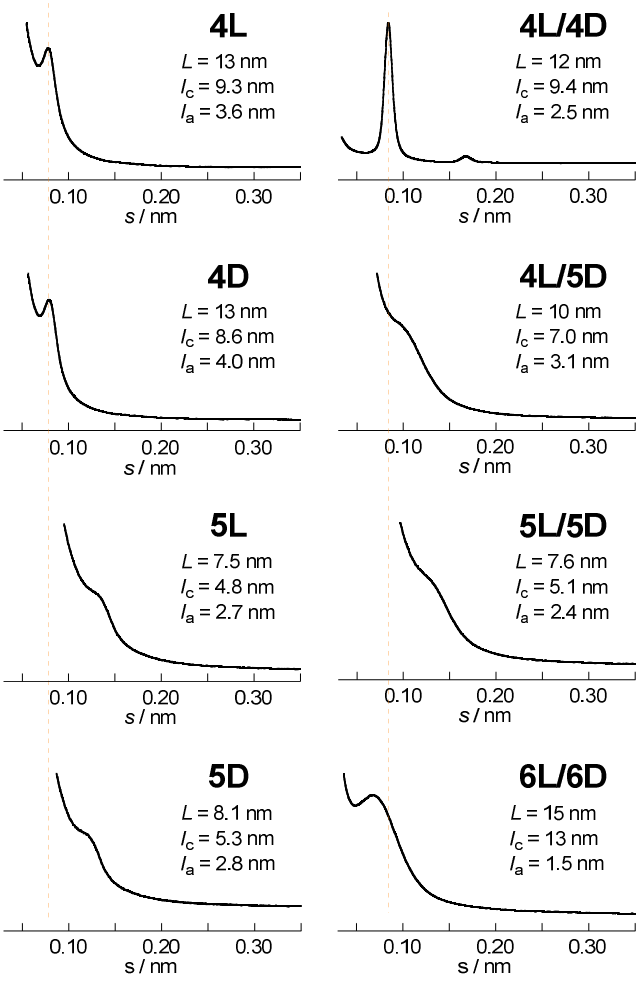

Figure 4. SAXS profiles of **4L**, **4D**, **5L**, **5D**, **4L/4D**, **4L/5D**, **5L/5D** and **6L/6D**.

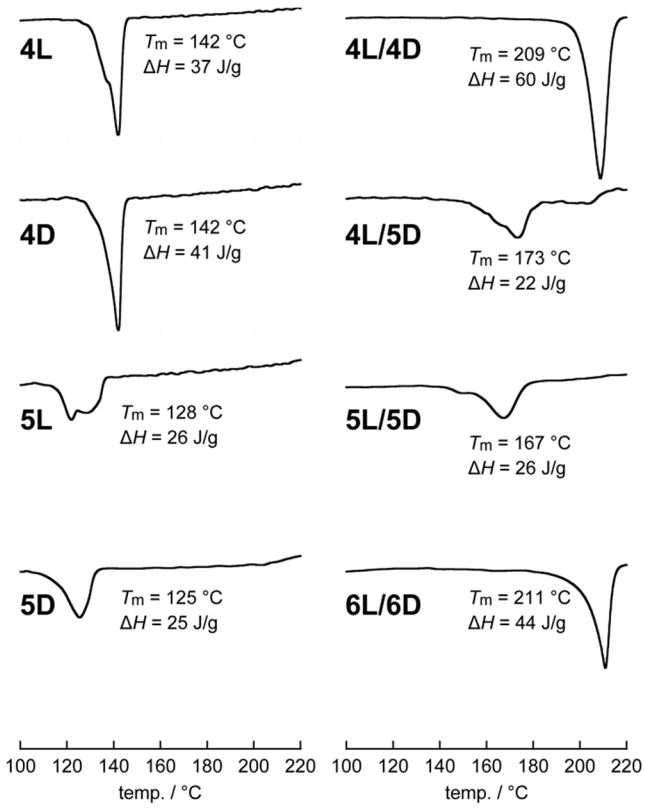

Figure 5. DSC thermograms of **4L**, **4D**, **5L**, **5D**, **4L/4D**, **4L/5D**, **5L/5D**, and **6L/6D**.

Table of contents entry

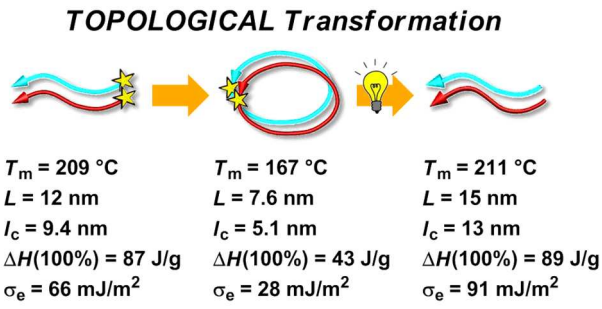

A new methodology for a stimuli-responsive polymer was proposed on the basis of cyclization and photocleavage. This requires only a single reaction per polymer molecule.